Mon. Not. R. Astron. Soc. **374,** 787–792 (2007) doi:10.1111/j.1365-2966.2006.11191.x

Chemical enrichment of the intracluster medium by FR II radio sources

D. Heath, M. Krause★ and P. Alexander
Astrophysics Group, Cavendish Laboratory, Cambridge CB3 0HE

Accepted 2006 October 11. Received 2006 October 10; in original form 2006 January 19

ABSTRACT

We present 2D axisymmetric hydrodynamic simulations investigating the long-term effect of Fanaroff–Riley type II radio galaxies on the metal distribution of the surrounding intracluster medium (ICM). A light jet is injected into a cooling flow atmosphere for 10–30 Myr. We then follow the subsequent evolution for 3 Gyr on a spherical grid spanning 3 Mpc in radius. A series of passive tracer particles were placed in an annulus about the cluster core to simulate metal carrying clouds in order to calculate the metallicity (Z) as a function of time and radial distance from the cluster centre. The jet has a significant effect on the ICM over the entire 3-Gyr period. By the end of the simulations, the jets produced metallicities of $\approx$10 per cent of the initial metallicity of the cluster core throughout much of the cluster. The jets transport the metals not only in mixing regions, but also through upwelling ICM behind the jet, enriching the cluster over both long and short distances.

Key words: hydrodynamics – methods: numerical – galaxies: jets.

1 INTRODUCTION

The intracluster gas has a metallicity of a third of the solar value ($Z_\odot$) on average (e.g. Molendi 2004; Renzini 2004), with values of $\approx 0.2\,Z_\odot$ up to the megaparsec scale. There is also evidence that the metals were expelled from the most massive galaxies in a cluster at redshifts $z > 1$ (Mushotzky & Loewenstein 1997) rather than being removed by ram pressure (Renzini 2004). The energy of the supernovae that produced these metals is hardly enough to expel the metals from the galaxies. An obvious alternative is radio sources produced by jets from the active galactic nuclei of giant ellipticals. Weak jets, as often found in nearby clusters, have been found inefficient in this respect (Brüggen 2002; Omma et al. 2004). Fanaroff–Riley type II (FR II) radio sources (Fanaroff & Riley 1974) are certainly powerful enough to do the job, especially at high redshift (e.g. Carilli et al. 2001). However, the actual mechanism by which the jets would do this is so far unclear.

It is becoming increasingly clear, from both observational and theoretical works, that radio sources have a significant impact on their environment. They push aside the intracluster gas, producing X-ray cavities (Carilli, Perley & Harris 1994; Alexander 2002; Smith et al. 2002; Zanni et al. 2003; Krause 2005; McNamara et al. 2005; Nulsen et al. 2005). The associated heating is relevant to the cooling flow problem (e.g. Kaiser & Alexander 1999; Kaiser & Binney 2003; Krause 2003). After the central engine has shut down, the low-entropy plasma that fills these cavities continues to rise through the surrounding atmospheres due to buoyancy and excess momentum (e.g. Churazov et al. 2001; Reynolds, Heinz & Begelman 2002; Kaiser 2003; Kaiser et al. 2005). This may lead to megaparsec scale convection, as demonstrated recently in 3D hydrodynamic simulations (Basson & Alexander 2003).

In the following, we investigate if this convection is able to eject the metals from a giant elliptical galaxy. We follow a similar approach to Basson & Alexander (2003), with the primary difference being the inclusion of tracer particles, to simulate metal containing clouds.

In contrast to previous work (Brüggen 2002; Omma et al. 2004), our approach is tailored for high-power FR II sources.

2 THE SIMULATIONS

The hydrodynamic simulations were constructed to model an FR II radio jet propagating through a cooling cluster atmosphere. The conservation equations for mass, momentum and energy were solved axisymmetrically, in two-dimensional spherical polar coordinates (r, θ), employing the FLASH code (Fryxell et al. 2000; Calder et al. 2002). FLASH is a conservative, adaptive-mesh hydrodynamics code using third-order interpolations. The simulated domain is a sphere with radius 3 Mpc, with a 20 kpc ($= r_{\rm inner}$) radius spherical cutout at the centre, with outflow boundary conditions (zero gradient, velocity unrestricted) set for when the jet is not active, allowing material to pass across it. The outer boundary at radius 3 Mpc is set to outflow also, so material can flow in from outside the simulation, whilst the $\theta = 0$ and $\theta = \pi$ boundaries are set to reflective to account for the rotational symmetry. The grid uses an adaptive mesh with a maximum of seven refinement levels to give effective maximum resolution of 6 and 0.1 kpc in the radial and angular directions, respectively; this gives up to 512 cells in both directions. The code employs square blocks of eight by eight cells. A typical distribution

★E-mail: M.Krause@mrao.cam.ac.uk

© 2006 The Authors. Journal compilation © 2006 RAS

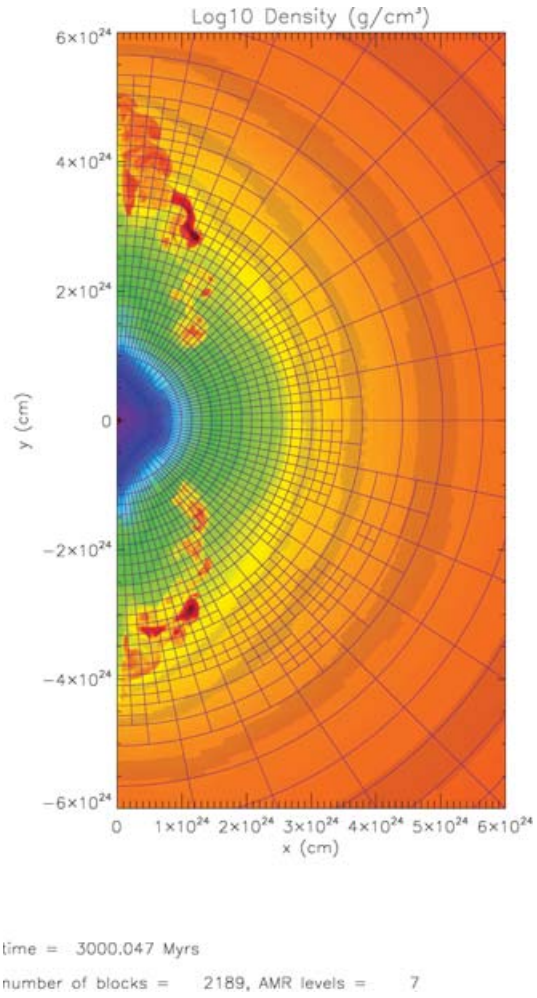

Figure 1. Block distribution for a typical run. Each block is resolved by 8×8 cells. The background displays the density, where the highest values are in the centre (2×10^{-24} kg m^{-3}, blue) and the lowest ones in the remains of the rising buoyant cocoon (2×10^{-28} kg m^{-3}, red). Only the central 2×4 Mpc of the 2D spherical grid is shown.

is shown in Fig. 1. The intracluster medium (ICM) was modelled as a monatomic, isothermal (10^8 K) King profile atmosphere, with a density profile given by

$$\rho_{\rm ICM} = \rho_0 \left[1 + (r/a_0)^2\right]^{-3\beta/2}, \quad (1)$$

where β was chosen to be 2/3 and the core radius (a_0) and core density (ρ_0) were 100 kpc and 10^{-23} kg m^{-3}, respectively. A gravitational acceleration of

$$g_r = -\frac{3\beta k_{\rm B} T}{\mu m_{\rm H} a_0^2} \frac{r}{\left[1 + (r/a_0)^2\right]} \quad (2)$$

towards the centre is used to keep the uncooled ICM in hydrostatic equilibrium, where $\mu = 1/2$, $\beta = 2/3$ and $m_{\rm H}$ is the mass of hydrogen. A bremsstrahlung cooling term (e.g. Longair 1994) was included of the form

$$\frac{{\rm d}E}{{\rm d}t} = 1.722 \times 10^{-40} n^2 \sqrt{T}\ {\rm W\,m^{-3}}, \quad (3)$$

assuming the ICM is comprised of ionized hydrogen and where n is the particle number density.

This setup was run for 200 Myr to allow an initial cooling flow to establish. To follow the distribution of metals $\approx 10^4$, passive tracer particles (chosen to obtain good statistics) were positioned between radii of 40 and 150 kpc from the cluster core so as to represent constant initial metallicity in the shell. The particles are introduced after 200 Myr, once the cooling flow is established – subsequently the particles move with the local velocity of the ICM.

Once the initial cooling flow has been established and particles added, the radio source is introduced by injecting low-density material across the inner ($r = 20$ kpc) boundary as two antiparallel jets in pressure equilibrium. Each jet has a half-opening angle of $\theta_{\rm open} = 0.5$ (=29°), and a velocity of $c/3$. The jets are therefore supersonic with respect to both the external and internal sound speed.

We present two simulations. They have the same total energy but differ in the instantaneous kinetic jet power, modelled by a trade-off between jet density and active time. Important parameters are shown in Table 1 for each run.

Table 1. Simulation parameters.

	$t_{\rm jet}$[a] (Myr)	$t_{\rm sim}$[b] (Myr)	$\rho_{\rm jet}$[c] (kg m^{-3})	$E_{\rm jet}$[d] (Joule)	$L_{\rm jet}$[e] (Watt)
Run A	10	3000	3×10^{-26}	3×10^{54}	4.7×10^{39}
Run B	30	3000	1×10^{-26}	3×10^{54}	1.6×10^{39}

[a] Jet's active time.
[b] Total simulation time.
[c] Mass density in the beam at inlet.
[d] Total energy released by both jets.
[e] Luminosity per jet, $L_{\rm jet} = \pi r_{\rm inner}^2\, \rho_{\rm jet}\, v_{\rm jet}^3\, (1 - \cos\theta_{\rm open})$.

3 RESULTS

Logarithmic density maps, including particle distribution, are shown in Figs 2 and 3. The general dynamics is very similar to that found by Basson & Alexander (2003). During the active phase, the jet develops the shock and cocoon structure that is typical for such simulations. After the jet activity has ceased, the centre quickly refills, and a convective flow establishes. The ICM flows outwards near the jet axis, and comes back near the equatorial regions.

3.1 Particle transport

The particles are not picked up by the bow shock, as one might naively have expected. This is easily explained by realizing that the front speed is generally larger than the gas velocities. The front therefore quickly passes, whereas gas and particles do not change their position significantly. The particles generally honour the contact surface, and are therefore displaced by the jet's cocoon. This can be observed early in the evolution and also in later phases (Figs 2 and 3) – this demonstrates the accuracy of the particle transport. The particles do enter intermediate density regions, where the jet plasma has mixed with the surrounding gas. As the simulation proceeds, instabilities cause the cocoon to lose its integrity and to 'dissolve' into a 'bubbly' structure. The tracer particles are found in the ICM gas between the bubbles, and as the turbulent structure rises buoyantly the tracer particles are dragged from the cluster core. At this time, we also see a large-scale convective flow established which is very similar to the one found by Basson & Alexander (2003). The particles are effectively entrained in the flow. In both simulations, the particles easily reach megaparsec scales at late times.

The particles show an artificial feature in the plane of symmetry. In the simulations presented here, there is very little asymmetry in the initial conditions. We also performed a simulation in which we

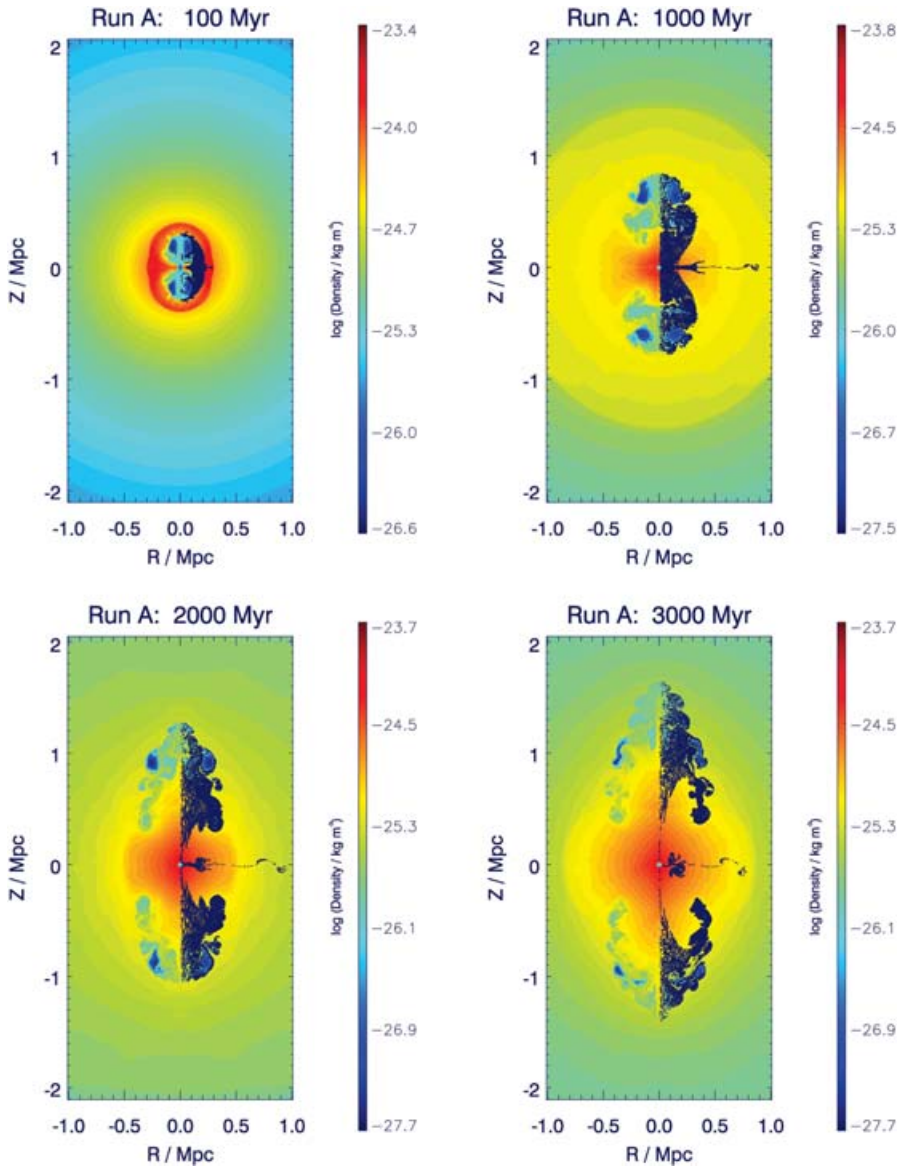

Figure 2. Logarithmic density maps for Run A at four times. Positions of the passive particles are overlaid on the right-hand side for each time.

introduced a significant asymmetry between the two jets, but which is in other respects identical to Run A – the feature in the symmetry plane is then strongly suppressed. About 10 per cent of the particles are in this feature, and it is significant in the region out to ≈100 kpc, only. About 1 per cent of the particles are lost across the inner radial boundary during the simulation.

Fig. 4 shows the final versus initial radii for all the surviving particles for Runs A and B. In both cases, most of the particles have been displaced by about a megaparsec. Their final position is independent of their initial position. We conclude that our results are likely to be insensitive to the precise initial distribution chosen for the tracer particles.

3.2 Metallicities

The tracer particles can be thought to represent a certain mass of metals, which can be assigned to each particle individually. In the following, we carry out a metallicity analysis with the initial 3D metallicity distribution normalized to be a constant in space. Since the initial particle distribution is homogeneous, the metal mass for each particle of the initial distribution is given by

$$M_{\rm particle} \propto \frac{\sin(\theta) r^2}{1 + (r/a_0)^2}. \quad (4)$$

This mass is a property of the particle and is retained as it moves during the simulation. In order to derive the metal mass in a given volume, we sum the contributions from every particle. For the metallicity in a 3D radial shell, this gives

$$Z \propto \frac{\sum_{\rm shell\ volume} M_{\rm particle}}{\int_{\rm shell\ volume} \rho \, {\rm d}V}. \quad (5)$$

Fig. 5 shows the time evolution of the metallicities relative to the initial core metallicity against radius for both runs. Due to the reduction of the core gas density, the metallicity first increases at small radii by a factor of a few and then decreases as the particles move outwards. In Run A, the central metallicity drops below its initial

© 2006 The Authors. Journal compilation © 2006 RAS, MNRAS **374,** 787–792

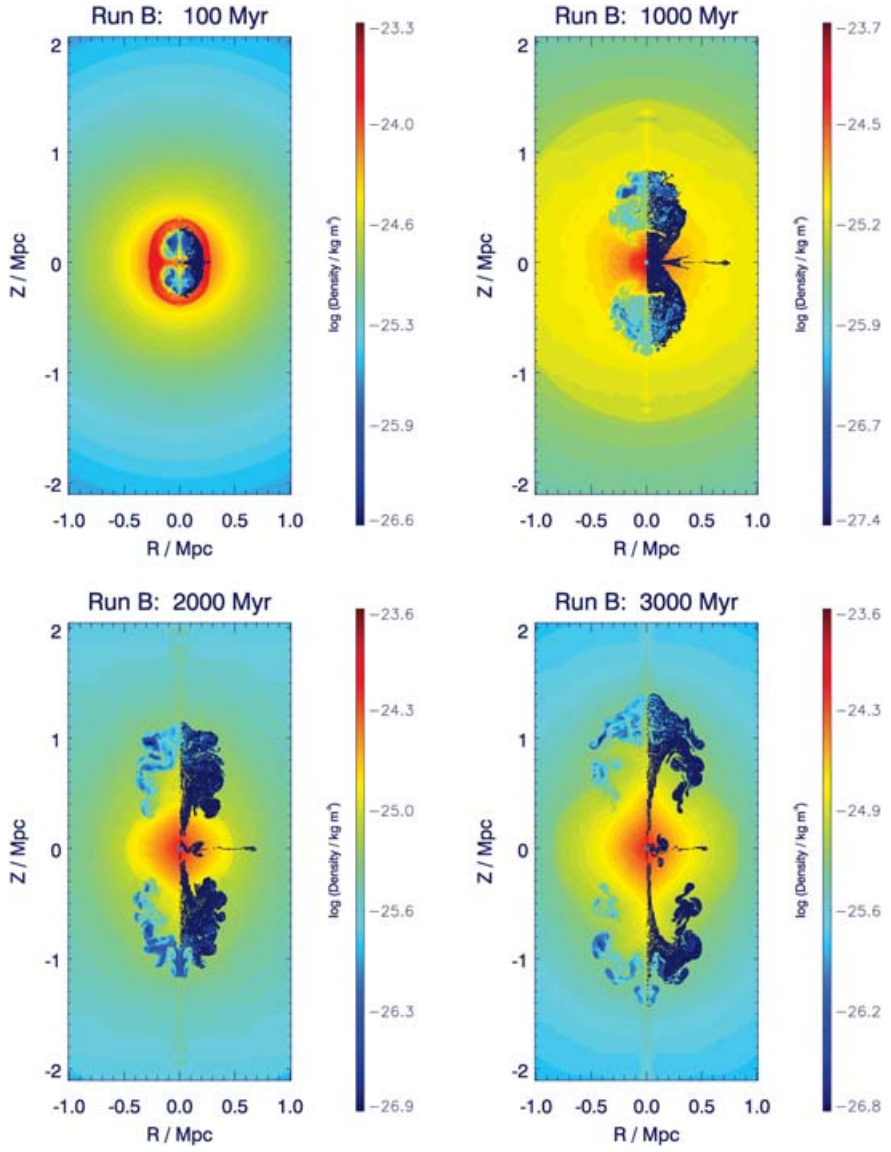

Figure 3. Same as Fig. 2, but for Run B.

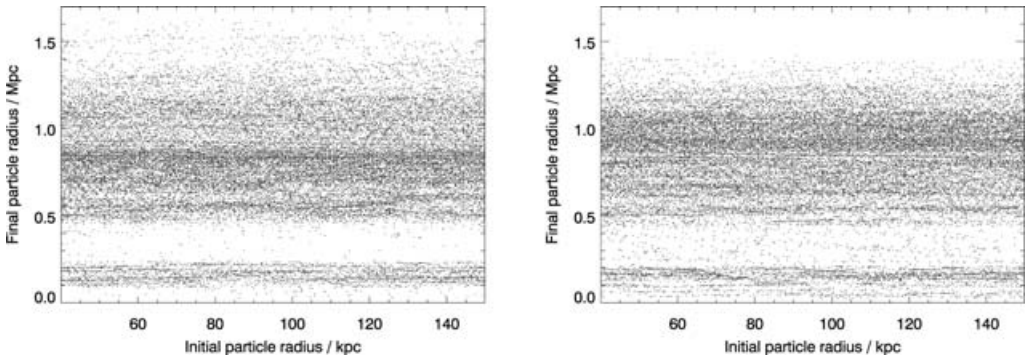

Figure 4. Final versus initial particle radii for Run A (left) and Run B (right).

value, whereas in Run B it stays above its initial value throughout the simulation. In both simulations, the metallicity reaches ≈5–10 per cent of the initial core metallicity on the megaparsec scale. The high-power jet (Run A) distributes the metals over a somewhat larger range out to larger radii than the lower power jet. The final metallicity distribution drops by a factor of 10 out to one megaparsec for Run A, and is almost constant between 0.4 and 0.8 Mpc for Run B.

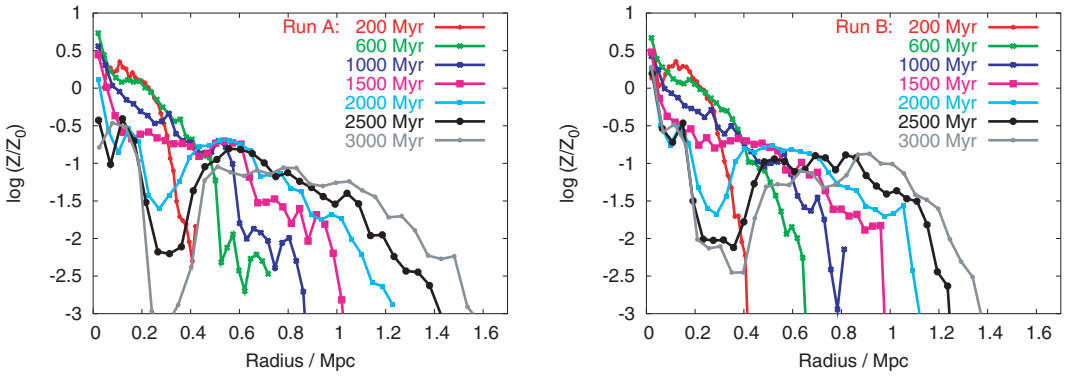

Figure 5. Derived metallicities for different simulation times for Run A (left) and Run B (right). The metallicities are normalized to the initial core metallicity. The symmetry feature (see the text) shows up in a narrow range around 100 kpc, for late times.

4 DISCUSSION

We have presented simulations of powerful jets which comprise an active phase as well as a phase long after the activity of the central source has ceased. Metal carrying clouds are simulated by a set of passive tracer particles. For the purpose of the present discussion, it is not relevant if the clouds remain intact or are instead dispersed, since we are only interested in the metallicity averaged over significant volumes. However, the cloud mass may be important. The energy to lift the clouds out of the cluster core comes from the kinetic energy of the convective flow. Hence, the mass of the clouds must be small compared to the total gas mass for our use of passive tracer particles to accurately represent the evolution of metallicity – this should be the case for realistic situations.

The particles are dragged out to the megaparsec scale by the large-scale convective flow and between the radio bubbles. Towards the end of the simulations, they occupy a linearly shaped region. The rising time-scale (Gyr) is of the order of the crossing time-scales for galaxies in the cluster. These will disperse the metals further. The same would be true for subcluster mergers. The exact metallicity distribution resulting from our simulations might therefore not be directly observable.

Quantitatively, the two runs differ slightly. Both simulated jets release the same total amount of energy. Run A, having a higher power but shorter active time, expels nearly all the tracer particles from the host galaxy, and distributes them to somewhat larger radii, with generally slightly smaller metallicity than in Run B.

This suggests that high-power sources might be more effective in the metal enrichment of clusters. Such sources are predominantly found at high redshift consistent with the observation that metal enrichment should have taken place at $z > 1$ (Mushotzky & Loewenstein 1997). The central metallicity gradient is quite different in Run A compared to Run B: in Run A the central metallicity profile is quite flat, while in Run B a steep central metallicity profile persists. Interestingly, observed cooling flow clusters show steep central metallicity gradients, while in non-cooling flow clusters it is rather flat. This has been explained by recent cluster mergers in the latter cases (De Grandi & Molendi 2001) and the absence thereof in the former. Our results suggest that only a fairly high power radio source flattens the metallicity gradients. Note that the radio sources at the centre of cooling flows in the local universe are almost exclusively of FR I type, i.e. they would have much lower power than the jets simulated here. Hence, we would not expect that they would erase central metallicity gradients. This is consistent with the findings of Brüggen (2002) and Omma et al. (2004), who simulate the metal evolution for low-power, subsonic flows. If a cluster would have produced a radio source with a power of more than 5×10^{39} W with a lifetime of about 10 Myr, within the preceding 2–3 Gyr, which is our simulation time, we would expect an effect on the central metallicity gradient. The time-scale is comparable to the time needed by the host galaxies to build up the metallicity gradients via stellar evolution (David et al. 2001; Wise, McNamara & Murray 2004), so the exact gradient would depend on the details.

Overall, the metallicities come close to 10 per cent of the initial core metallicity. Therefore, depending on the metallicities in the host galaxy, one outburst might already produce a significant fraction of the metals observed in present day clusters.

Although the presented simulations are 2D axisymmetric, we expect the simulations to recover the basic trends from full 3D simulations, since computations similar to those presented here have already been performed in 3D (Basson & Alexander 2003), and a very similar overall flow structure has been reported. A significant magnetic field would change the details of the mixing between the jet plasma and the cluster gas but could hardly influence the large-scale flow structure.

5 CONCLUSIONS

We have shown that the remnants of powerful FR II jets can efficiently drag passive tracer particles out of the host galaxy. These particles are a good representation of metal containing clouds as long as the total mass of the clouds is small compared to the gas mass of the galaxy cluster. The resulting metallicity distribution was very shallow with gas on the megaparsec scale reaching metallicities of up to 10 per cent the initial metallicity of the cluster core. The angular metallicity distribution is peaked towards the former jet axis. Neglected processes in the cluster are expected to produce a more isotropic distribution. Observations generally show a homogeneous metallicity distribution, with values of about $Z_{\odot}/3$, constant out to large radii. The metals are believed to originate predominantly from the largest cluster members, having been expelled at redshift $z > 1$. Powerful jets are detected out to much higher redshifts, and are believed to originate in the most massive galaxies at their redshift. As we have shown here, their remnants are able to expel metals from their host galaxy and distribute them throughout the galaxy cluster. This provides additional evidence that FR II radio jets may contribute significantly to the metal transport in galaxy clusters.

© 2006 The Authors. Journal compilation © 2006 RAS, MNRAS **374,** 787–792

ACKNOWLEDGMENTS

The software used in this work was in part developed by the DOE-supported ASC/Alliance Center for Astrophysical Thermonuclear Flashes at the University of Chicago. MK acknowledges support through a fellowship (Kr 2857/1-1) of the Deutsche Forschungsgemeinschaft (DFG).

REFERENCES

Alexander P., 2002, MNRAS, 335, 610
Basson J. F., Alexander P., 2003, MNRAS, 339, 353
Brüggen M., 2002, ApJ, 571, L13
Calder A. C. et al., 2002, ApJS, 143, 201
Carilli C. L., Perley R. A., Harris D. E., 1994, MNRAS, 270, 173
Carilli C. L. et al., 2001, in Hibbard J. E., Rupen M., van Gorkom J. H., eds, ASP Conf. Ser. Vol. 240, Gas and Galaxy Evolution. Astron. Soc. Pac., San Francisco
Churazov E., Brüggen M., Kaiser C. R., Böhringer H., Forman W., 2001, ApJ, 554, 261
David L. P., Nulsen P. E. J., McNamara B. R., Forman W., Jones C., Ponman T., Robertson B., Wise M., 2001, ApJ, 557, 546
De Grandi S., Molendi S., 2001, ApJ, 551, 153
Fanaroff B. L., Riley J. M., 1974, MNRAS, 167, 31
Fryxell B. et al., 2000, ApJS, 131, 273
Kaiser C. R., 2003, MNRAS, 343, 1319
Kaiser C. R., Alexander P., 1999, MNRAS, 305, 707
Kaiser C. R., Binney J., 2003, MNRAS, 338, 837
Kaiser C. R., Pavlovski G., Pope E. C. D., Fangohr H., 2005, MNRAS, 359, 493
Krause M., 2003, A&A, 398, 113
Krause M., 2005, A&A, 431, 45
Longair M. S., 1994, High Energy Astrophysics, Vol. 2. Cambridge Univ. Press, Cambridge
McNamara B. R., Nulsen P. E. J., Wise M. W., Rafferty D. A., Carilli C., Sarazin C. L., Blanton E. L., 2005, Nat, 433, 45
Molendi S., 2004, in Bertin G., Farina D., Pozzoli R., eds, AIP Conf. Proc. 703, Plasmas in the Laboratory and in the Universe: New Insights and New Challenges. Am. Inst. Phys., Melville, p. 345
Mushotzky R. F., Loewenstein M., 1997, ApJ, 481, L63
Nulsen P. E. J., Hambrick D. C., McNamara B. R., Rafferty D., Birzan L., Wise M. W., David L. P., 2005, ApJ, 625, L9
Omma H., Binney J., Bryan G., Slyz A., 2002, MNRAS, 332, 271
Renzini A., 2004, in Mulchaey J. S., Dressler A., Oemler A., eds, Clusters of Galaxies: Probes of Cosmological Structure and Galaxy Evolution. Cambridge Univ. Press, Cambridge, p. 261
Reynolds C. S., Heinz S., Begelman M. C., 2002, MNRAS, 332, 271
Smith D. A., Wilson A. S., Arnaud K. A., Terashima Y., Young A. J., 2002, ApJ, 565, 195
Wise M. W., McNamara B. R., Murray S. S., 2004, ApJ, 601, 184
Zanni C., Bodo G., Rossi P., Massaglia S., Durbala A., Ferrari A., 2003, A&A, 402, 949

This paper has been typeset from a TEX/LATEX file prepared by the author.